Design of Janus Nanoparticles with Atomic Precision: Tungsten-Doped Gold Nanostructures

Qiang Sun,[†,‡,∥,*] Qian Wang,[§,‡] Puru Jena,[‡] and Yoshiyuki Kawazoe[⊥]

[†]Department of Advanced Materials and Nanotechnology, Peking University, Beijing 100871, China, [‡]Physics Department, Virginia Commonwealth University, Richmond, Virginia 23284, [§]School of Physical Science and Technology, Southwest University, Chongqing 40071, China, [⊥]Institute for Materials Research, Tohoku University, Sendai 980-77, Japan, and [∥]Center for Applied Physics and Technology, Peking University, Beijing 100871, China

ABSTRACT Janus nanoparticles, characterized by their anisotropic structure and interactions, have added a new dimension to nanoscience because of their potential applications in biomedicine, sensors, catalysis, and assembled materials. The technological applications of these nanoparticles, however, have been limited as the current chemical, physical, and biosynthetic methods lack sufficient size and shape selectivity. We report a technique where gold clusters doped with tungsten can serve as a seed that facilitates the natural growth of anisotropic nanostructures whose size and shape can be controlled with atomic precision. Using *ab initio* simulated annealing and molecular dynamics calculations on Au_nW ($n > 12$) clusters, we discovered that the $W@Au_{12}$ cage cluster forms a very stable core with the remaining Au atoms forming patchy structures on its surface. The anisotropic geometry gives rise to anisotropies in vibrational spectra, charge distributions, electronic structures, and reactivity, thus making it useful to have dual functionalities. In particular, the core−patch structure is shown to possess a hydrophilic head and a hydrophobic tail. The $W@Au_{12}$ clusters can also be used as building blocks of a nanoring with novel properties.

KEYWORDS: nanoanisotropy · multifunction · Janus structure · magic cluster · stability

Nanoparticles with their unusual properties have ushered in a new era in materials science. The reduced size, coordination, and dimensionality of these nanoparticles allow the synthesis of a new class of materials with tailored properties. Because of the minimization of the surface tension energy, the nanoparticles are typically spherical in shape with isotropic distribution of charge densities. Recently, a great deal of interest has been given to the shape-controlled synthesis[1−6] of nanostructures with anisotropies that possess certain advantages over their spherical counterparts. These include molecular recognition, self-assembly, and generation of highly ordered lattices such as photonic crystals. In 1992 De Gennes used the term Janus[7] after the Roman God Janus, to describe these particles. Like the God, Janus who is described as having two heads, the two hemispheres of the Janus particles have different chemical character and hence can be dually functionalized for potential applications in medical therapeutics, wavelength-sensitive window coatings, and biodiagnostic chemistry. While several techniques[8−14] such as electrochemical and photochemical reduction, templating of porous membranes and nanotubes, and surfactant-aided growth are available for the fabrication of these anisotropic particles, due to the complicated nucleation and growth process it is difficult to control their size and morphology. In this article we prescribe a technique where Janus nanoparticles with atomic precision and morphology can be synthesized in the gas phase. We demonstrate this route by considering tungsten-doped gold clusters.

The current interest in gold nanostructures[15−29] stems from their extensive potential applications in catalysis, microelectronics, and biomedicine. It is highly desirable to introduce Janus anisotropy into gold nanostructures, so that they can have dual functionality for some new applications, such as carrying two different or complementary medicines, sensing two different molecules, or simultaneously catalyzing two different reactions. Tungsten, with its high melting point and high tensile strength, is widely used as a doping agent to change or improve the functions and performance of materials such as sintering, microstructure, dielectric properties, and ferroelectric properties. In particular, tungsten doping and alloying have been widely used in the gold jewelry industry for modulating malleability and ductility. Gold−tungsten composite materials are also used for microwave power transistors.

The large surface area of gold nanostructures offers the added flexibility that doping with W can have a bigger impact on

*Address correspondence to sunq@coe.pku.edu.cn, qsun@vcu.edu.

Received for review September 29, 2007 and accepted December 19, 2007.

Published online January 19, 2008. 10.1021/nn7002647 CCC: $40.75

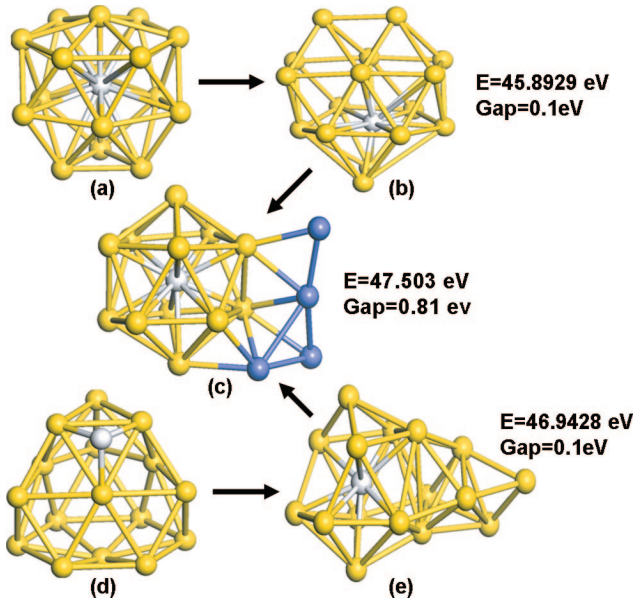

Figure 1. Geometry evolution of $Au_{16}W \rightarrow (Au_{12}W)Au_4$. The Au atoms forming a patch are plotted in gray in the final structure (c).

their structure and properties than those in bulk Au. The open questions are: How does the geometry of the Au nanoclusters change upon doping? Is there a general pattern that could describe this change? How does doping affect the electronic properties? To answer these questions, we have concentrated on three different clusters, Au_{16}, Au_{20}, and $Au_{32}$for the following reasons: (1) Au_{16} is one of the few metal clusters that has been experimentally verified to form a cage structure.[15] With a diameter of about 5 Å, this cage is large enough to accommodate an endohedral atom. A fascinating application of this cage is that it can be used as a nanocarrier of drugs. (2) Au_{20} is well-known for its pyramidal geometry,[16] large HOMO–LUMO gap (1.770 eV) comparable to that of C_{60}, and packing consistent with the Au(111) surface. It is interesting to know how doping of W would affect this stable structure. (3) The cage structure of Au_{32} has recently been shown to be unstable.[17] Can it be stabilized by doping with W? Note that $W@Au_{12}$ has been known to be a magic cluster

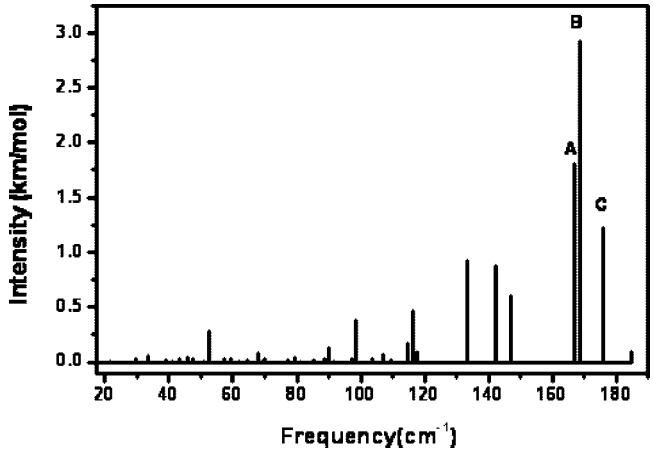

Figure 2. Vibrational spectra of $(Au_{12}W)Au_4$.

where W atom resides inside the icosahedral cage of Au_{12}, and the extraordinary stability arises due to the 18-electron rule (12 electrons from 12 Au atoms and 6 electrons from W).[30–33]

In this article, we not only provide answers to these questions for the first time but also introduce an entirely new class of lowest energy structures where all the Au_nW (n = 16, 20, and 32) clusters exhibit anisotropic shape and charge densities consistent with Janus structures. The anisotropy results because the $W@Au_{12}$ cluster is unusually stable due to the 18-electron rule. In the growth of WAu_n clusters with $n > 12$, $W@Au_{12}$ forms a stable core while the extra Au atoms segregate on one side of the cluster forming a patchy structure. These results suggest a novel technique for the synthesis of Janus nanoparticles whose composition and shape can be controlled at the atomic level. Equally important, these particles can have dual functionalities.

$Au_{16}W$ Cluster. We begin with the Au_{16} cage structure shown in Figure 1a. Optimization was carried out by first putting the W atom inside the Au_{16} cage. The resulting geometry is shown in Figure 1b where the W atom is found to shift to an off-center position. The total binding energy of this complex is 45.8929 eV with an energy gap of 0.1 eV between the highest occupied molecular orbital (HOMO) and the lowest unoccupied molecular orbital (LUMO). To further study the stability of this off-center configuration, we carried out simulated annealing. After 15 ps the structure in Figure 1b transformed to that in Figure 1c. This structure is composed of a $Au_{12}W$ core with the W atom embedded inside the Au_{12} icosahedric cage. The reamining four Au atoms (indicated in gray) form a patchy structure attached to the core surface. The total binding energy of $Au_{16}W$ in Figure 1c is 47.503 eV and the HOMO–LUMO gap increased from 0.1 eV in Figure 1b to 0.81 eV. The stability of this patchy structure suggests that the magic $W@Au_{12}$ cluster serves as the building block for the growth of larger W-doped Au clusters.

An interesting question now arises: How does the W atom enter into the cage once the Au_{16} cluster is formed? Note that the cage surface of Au_{16} is composed of 28 triangles. We started the optimization process by placing the W atom on one of the triangular faces (Figure 1d). The surface modified by opening a pentagon through which the W atom entered into the cage (Figure 1e). Compared to the structure in Figure 1b, this distorted structure is more stable in energy by about 1.05 eV. Starting with this structure, we performed a simulated annealing. After 15 ps simulation the geometry was found to converge to the patchy structure shown in (Figure 1c). Thus, we confirmed that the structural transition of $W@Au_{16} \rightarrow (Au_{12}W)Au_4$ is due to the unusual stability of the $Au_{12}W$ cluster. To further check the stability of $(Au_{12}W)Au_4$, frequency calculations were carried out. All the 45 vibrational modes have no imaginary components, suggesting that this

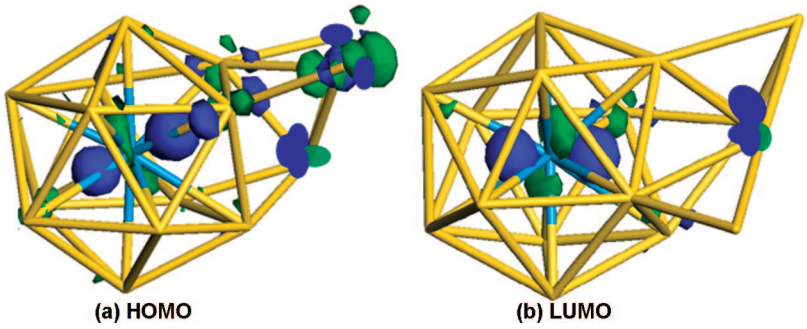

Figure 3. HOMO and LUMO obitals of $Au_{16}W$.

core−patch structure is dynamically stable. The vibrational spectrum is given in Figure 2, where three modes with high peaks in intensity are labeled as A, B, and C, respectively. The modes of A and C are mainly contributed by the motions of the W atom, while the mode B with the greatest intensity is mainly derived from the vibrations of Au atoms in the patch. So this core−patch structure is anisotropic not only in geometry but also in vibrational properties.

To demonstrate the anisotropy in electronic structure, we have plotted the HOMO–LUMO orbitals of Figure 1c in Figure 3. The LUMO is mainly derived from the endohedral W atom, while the major contribution to HOMO comes from the W atom as well as the Au atoms in the patch. This suggests that the Au atoms in the patch can be more reactive than the other Au atoms forming the core of $W@Au_{12}$. Consequently W doping also introduces anisotropy in chemical reactivity of $Au_{16}W$ allowing the possibility that this nanostructure can have dual functionalities. On the basis of the anisotropies exhibited in geometry, vibration, and electronic structure, we can identify this core−patch structure $(Au_{12}W)Au_4$ as a Janus equivalent.

$Au_{20}W$ Cluster. Next we studied the interaction of Au_{20} with a W atom. The surface of Au_{20} consists of 40 triangles.[16] We introduced a W atom on one of these triangles, as shown in Figure 4, panel a. After optimization, the original face-centered cubic (fcc)(111)-like surface of Au_{20} reconstructed with a hexagonal opening around the W atom (Figure 4b). The corresponding total binding energy of $Au_{20}W$ in Figure 4b is 56.7731 eV with a small HOMO–LUMO gap of 0.03 eV. Starting with this structure, simulated annealing was carried out. After 15 ps the geometry relaxed to that given in Figure 4c. Once again the core−patch type structure appears with $W@Au_{12}$ as the core. The remaining eight Au atoms (shown in gray) form a patch capped onto the core surface. Compared to the structure in Figure 4b, the total binding energy of Figure 4c is lowered by 1.334 eV, and the HOMO–LUMO gap is increased to 1.02 eV. The corresponding HOMO and LUMO orbitals are given in panels a and b of Figure 5, respectively. Note that these orbitals share similar features with that of $Au_{16}W$ in Figure 3. Thus, Au atoms forming the patchy structure are expected to show different chemical activity than those forming the core structure.

$Au_{32}W$ Cluster. The last example of a W-doped Au cluster we have considered is $Au_{32}W$. This choice was made for the following reason. We recall that $W@Au_{12}$, due to the 18-electron rule, is a very stable cluster and, as we have seen in the last two examples, it forms the building block for the larger Au clusters ($Au_{16}W$ and $Au_{20}W$). We further note that the icosahedric $W@Au_{12}$ cluster has 20 triangular faces on its surface and capping this surface with 20 additional Au atoms would form a cluster of $Au_{32}W$. This structure is shown in Figure 6a where the Au atoms in the second shell are marked in gray. Intuitively, this structure should be stable as it constitutes a stable $W@Au_{12}$ core and the 20 Au atoms on its surface can add further stability by contributing 20 electrons, enough to close electronic shells. Note that the unusual stability of simple metal clusters containing enough electrons (2, 8, 20, 40, . . .) to close electronic shells was demonstrated by Knight and co-workers[34] in terms of a jellium model. Thus, by coating the $W@Au_{12}$ magic cluster with 20 Au atoms, one could arrive at a doubly magic cluster. This is analogous to doubly magic nuclei whose existence has been known for quite some time.[35] It is also interesting to note that the cage structure of Au_{32} has been recently found to be unstable.[17] Now the question is: Can $W@Au_{12}$ act as an endohedral core to stabilize a cagelike structure of gold?

Following the similar procedure of simulated annealing described earlier, we found that the struc-

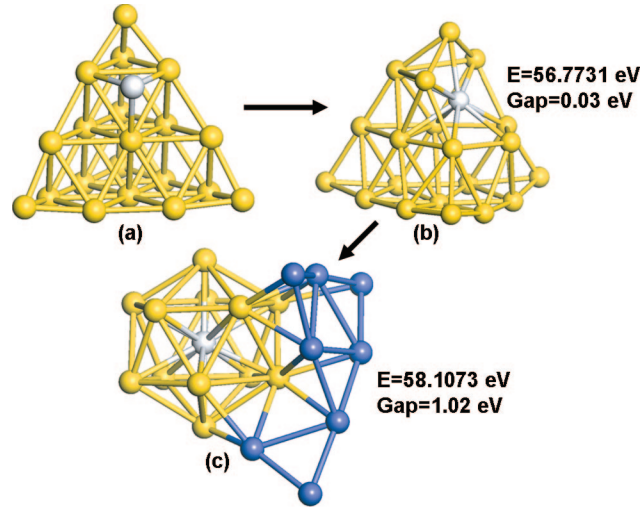

Figure 4. Geometry evolution of $WAu_{20} \rightarrow (Au_{12}W)Au_8$. The atoms forming in the patch are plotted in gray.

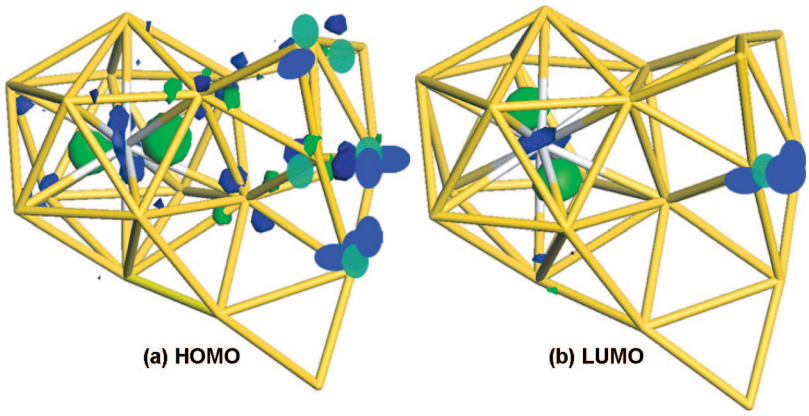

Figure 5. HOMO and LUMO obitals of WAu_{20}.

ture of $Au_{32}W$ is that of a $W@Au_{12}$ core with the remaining 20 Au atoms segregating on the outer shell to form a patchy structure. We show two views of this structure in Figure 6, panels b and c. The packing pattern in the patch can be clearly seen to resemble the fcc-(111) structure. So the stable $W@Au_{12}$ core together with the closed-packing patch makes this geometry stable. The HOMO–LUMO gap of this structure is of 0.57 eV. The core−patch structure in $Au_{32}W$ is consistent with what we found in $Au_{16}W$ and $Au_{20}W$. At this size, the anisotropy in geometry results in increasing anisotropy of the electronic structure. This can be seen from the HOMO and LUMO orbitals plotted in Figure 7. Especially from the LUMO we can find that the patch is more reactive than the core. This would provide a very unique way to selectively functionalize this nanostructure with dual functionality that is the hallmark of Janus nanoparticles.

Gold is the most electronegative metal, comparable to selenium, and only slightly more electropositive than sulfur and iodine. Therefore, it can form compounds such as $Au^{-}Cs^{+}$ where gold is anionic. When a W atom is doped into Au_n, charge transfer takes place. In the stable core−patch structure of $(Au_{12}W)Au_x$, the transferred charges are mainly distributed in the core part. This results in a dipole moment of 2.38 D in $(Au_{12}W)Au_{20}$. The imbalance in charge distribution in the core−patch structure brings some interesting features. For example, because the Au atoms in the core part are negatively charged, when water molecules are introduced to this core part, the Coulomb repulsion would exist between the electron lone pairs in water molecule and negative charges of Au atoms in the core part. This would make the core part hydrophobic, while the patch part would become hydrophilic. To confirm this idea, we placed two water molecules at opposite ends in Figure 8. Structure optimization indicates that the water molecule at pole A flies away from the core, while the water molecule at pole B is adsorbed at a distance of 2.22 Å from the patch. The corresponding adsorption energy is 0.19 eV. Therefore the core−patch structure has a hydrophobic head and a hydrophilic tail, which represents a unique nanoscale analogue of the conventional surfactant molecules, exhibiting hydrophobic characters on one side and hydrophilic characters on the other. Recently, Kumacheva and coworkers used more complicated methods to selectively functionalize the ends of hydrophilic gold nanorods with hydrophobic polymers to make them amphiphilic, resulting in two-dimensional solvent-dependent organization.[36,37]

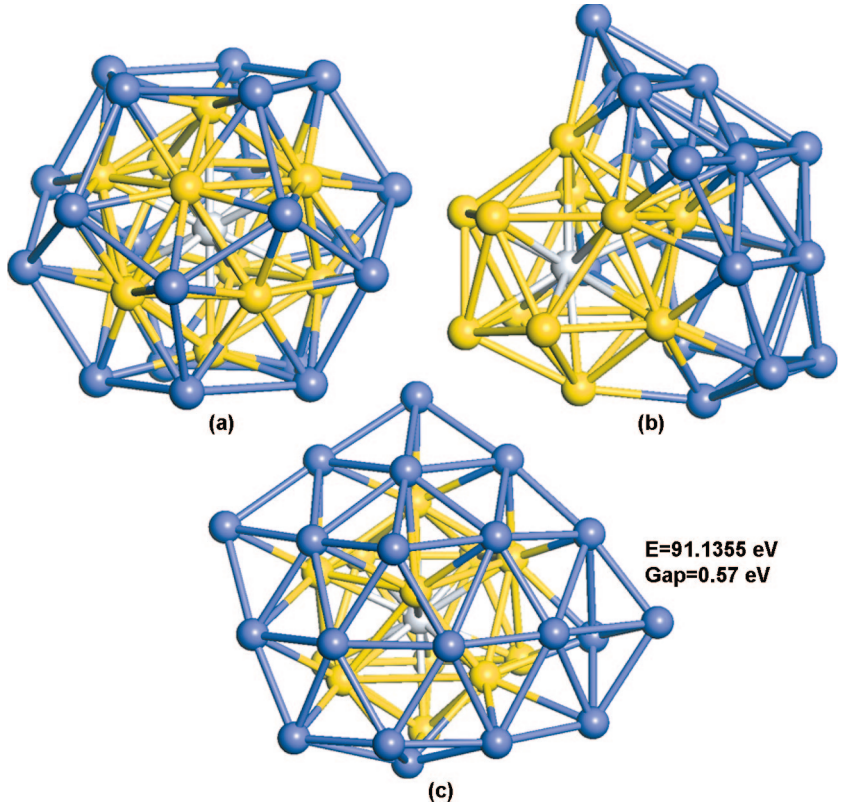

Figure 6. Geometry evolution of $WAu_{32} \rightarrow (Au_{12}W)Au_{20}$. The initial geometry is shown in panel a and the side and top views of the final optimized geometry are shown in panels b and c, respectively. The atoms in the patch are in gray.

A Nanoring Composed of $Au_{12}W$ as a Building Block. From the structures of $Au_{16}W$, $Au_{20}W$, and $Au_{32}W$, we see that $W@Au_{12}$ always forms a stable core onto which the remaining Au atoms are grafted. This suggests that $W@Au_{12}$ cluster can be used a building block for a variety of nanostruc-

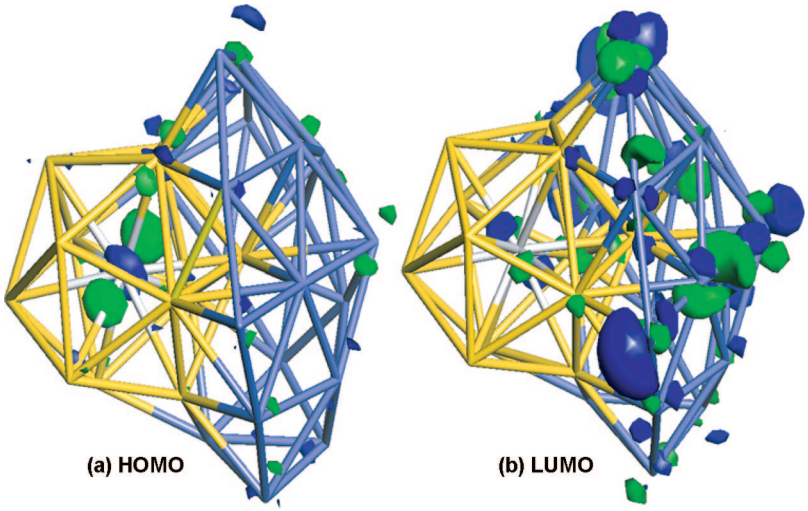

Figure 7. HOMO and LUMO obitals of WAu_{32}.

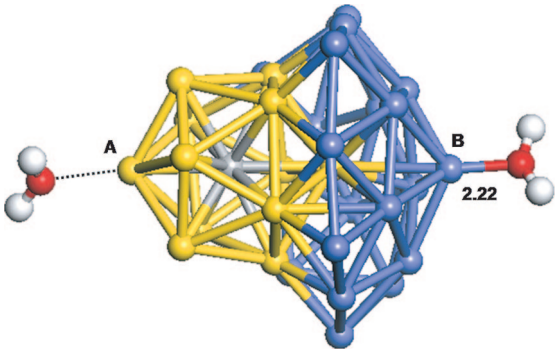

Figure 8. Water molecules in $(Au_{12}W)Au_{20}$ with the hydrophobic core (in yellow) and hydrophilic patch (in gray).

tures, which would have some interesting geometries and properties.[38,39] Here we study a nanoring composed of nine units of $W@Au_{12}$ by allowing them to share a triangle surface with each other as shown in Figure 9, panels a and b. We carried out molecular dynamics simulation by using Nose algorithm[40] at $T = 300$ K for 15 ps with a time step of 1 fs. The resulting geometry, shown in Figure 9c was found to be very stable with the total binding energy of 293.8877 eV. In Figure 9d we plot the charge density difference, defined as the difference between the total electron density of the nanoring and that of the isolated atoms. We can clearly see that the charges accumulate on the bonds, showing a covalent bonding feature in this cluster assembled nanoring structure.

It is interesting to note that the charge distribution in this nanoring is also anisotropic, where the Au atoms in the outer ring carry more charges than those in the inner ring. Thus the outer ring behaves more hydrophobic than the inner ring. However, the net dipole moment of the whole ring is zero due to its symmetric geometry, different from the core−patch structure discussed above. The anisotropy also exists in the electronic structure. The HOMO of this nanoring mainly originates from the W atoms, while the LUMO is predominantly derived from W atoms as well as the outermost part of the ring, as shown in Figure 10. In this case, the outer ring is much more reactive than the inner ring. Therefore, this stable nanoring also displays Janus anisotropy in electronic structure, charge distribution, and chemical activity.

Summary. Extensive simulations based on first principles techniques have resulted in some very interesting predictions: (1) Inherent stability of $W@Au_{12}$ cluster derived from the 18-electron rule permits this cluster to act as a building block for larger W-doped Au clusters and introduces anisotropy in the structures naturally. (2) The anisotropic structures of these clusters originate when the remaining Au atoms form a patchy structure on the $W@Au_{12}$ surface. (3) These structures are characteristic of Janus nanoparticles and exhibit anisotropic electronic structure, vibrational spectra, and reactivity. The charges transferred from the W atom are mainly localized on the core part, making the core hydrophobic and the patch hydrophilic. Thus, the nanoclusters can

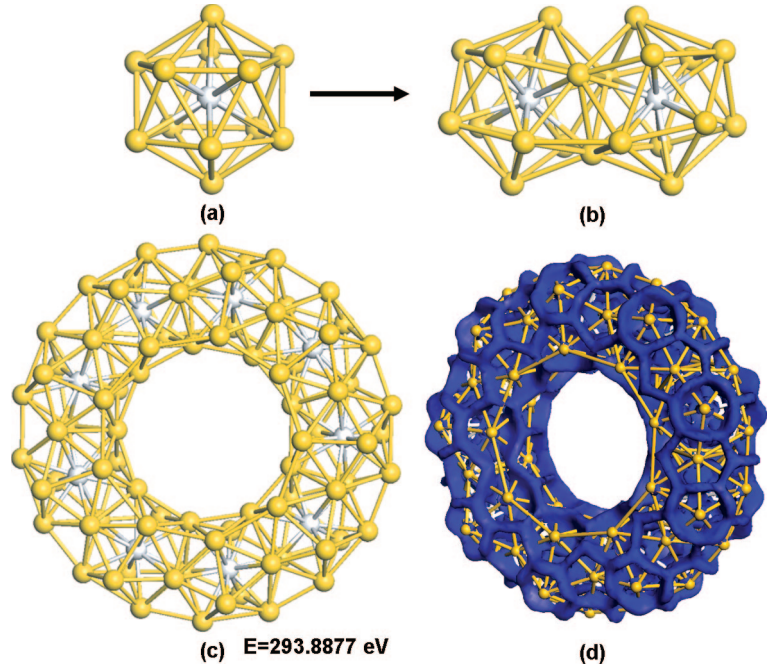

Figure 9. $W@Au_{12}$ cluster assembled nanoring: a) $W@Au_{12}$ building block; b) W_2Au_{21} and c) W_9Au_{81} nanoring; d) the charge difference isosurface plot of the nano ring.

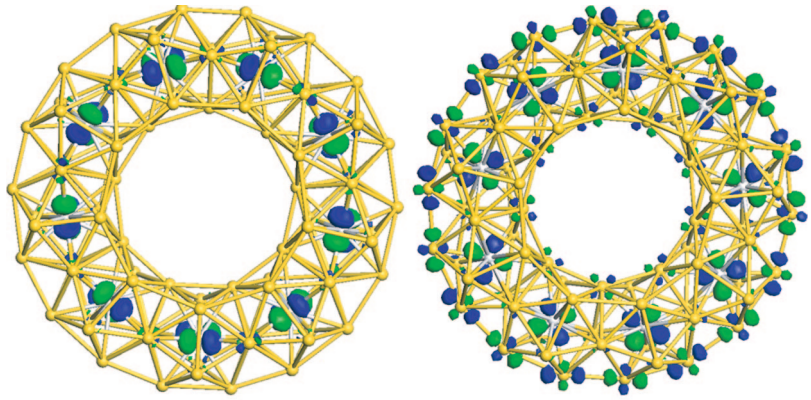

Figure 10. HOMO and LUMO of W_9Au_{81} nanoring.

have dual functionalities. (4) The stable $W@Au_{12}$ clusters can also be used to form a ring structure where their individual structural identity is maintained. More importantly, the electron distributions of the outer and inner ring surfaces are different and thus this nanoring can also be used for dual functions. Therefore, W doping provides a simple and effective method for introducing Janus anisotropy in the structure, charge distribution, vibration, electronic structure, and reactivity. By use of gas phase techniques these Janus-like gold nanostructures can be synthesized with atomic precision. Such structures can have many possible applications in technology as Au can be easily functionalized. We hope that our work will stimulate synthesis of Janus nanostructures in the gas phase.

METHODS

Our results are based on spin-polarized density functional calculations with generalized gradient approximation (GGA) for exchange and correlation potential. We have used the PBE form for the GGA and a plane-wave basis set with the projector augmented plane wave (PAW) method as implemented in the Vienna *ab Initio* Simulation Package (VASP).[41,42] Supercells with 15 Å vacuum spaces along *x*, *y*, and *z* directions for all the calculated structures are used. Due to the large supercell the Γ point is used to represent the Brillouin zone. The geometries of the structures are first optimized at 0 K without any symmetry constraint. The energy cutoff was set to 380 eV and the convergence in energy and force were 10^{-4} eV and 1×10^{-3} eV/Å, respectively. The accuracy of our numerical procedure has been well tested in our previous studies for Au and W−Au systems.[43–45] Starting with the optimized structures obtained from the above, molecular dynamics calculations with simulated annealing were performed from 800 to 0 K with a time step of 1 fs to locate the global equilibrium structure.

Acknowledgment. This work is partly supported by Peking University and the US Department of Energy. Q.S. thanks Gang Chen for discussions. The authors thank the crew of the Center for Computational Materials Science, the Institute for Materials Research, Tohoku University, for their continuous support of the HITAC SR11000 supercomputing facility. The authors also thank the reviewers for their time and comments.

REFERENCES AND NOTES

1. Klajn, R.; Bishop, K. J. M.; Fialkowski, M.; Paszewski, M.; Campbell, C. J.; Gray, T. P.; Grzybowski, B. A. Plastic and Moldable Metals by Self-Assembly of Sticky Nanoparticle Aggregates. *Science* **2007**, *316*, 261–264.
2. Glotzer, S. C.; Solomon, M. J. Anisotropy of Building Blocks and Their Assembly into Complex Structures. *Nat. Mater.* **2007**, *6*, 557–562.
3. Shevchenko, E. V.; Talapin, D. V.; Kotov, N. A.; O'Brien, S.; Murray, C. B. Structural Diversity in Binary Nanoparticle Superlattices. *Nature* **2006**, *439*, 55–59.
4. Blaaderen, A. V. Materials Science: Colloids Get Complex. *Nature* **2006**, *439*, 545.
5. Leunissen, M. E. Nanotechnology: Nano-Oscillators Get It Together. *Nature* **2005**, *437*, 325–326.
6. Roh, K-H.; Matin, D. C.; Lahann, J. Biphasic Janus Particles with Nanoscale Anisotropy. *Nat. Mater.* **2005**, *4*, 759–763.
7. De Gennes, P. G. Soft Matter. *Rev. Mod. Phys.* **1992**, *64*, 645–648.
8. Nisisako, T.; Torii, T. Formation of Biphasic Janus Droplets in a Microfabricated Channel for the Synthesis of Shape-Controlled Polymer Microparticles. *Adv. Mater.* **2007**, *19*, 1489–1493.
9. Walther, A.; Andre, X.; Drechsler, M.; Abetz, V.; Muller, A. H. E. Janus Discs. *J. Am. Chem. Soc.* **2007**, *129*, 6187–6198.
10. Nie, Z.; Li, W.; Seo, M.; Xu, S.; Kumacheva, E. Janus and Ternary Particles Generated by Microfluidic Synthesis: Design, Synthesis, and Self-Assembly. *J. Am. Chem. Soc.* **2006**, *128*, 9408–4912.
11. Nisisako, T.; Torii, T.; Takahashi, T. Synthesis of Monodisperse Bicolored Janus Particles with Electrical Anisotropy Using a Microfluidic Co-Flow System. *Adv. Mater.* **2006**, *18*, 1152–1156.
12. Perro, A.; Reculusa, S.; Ravaine, S.; Bourgeat-Lami, E.; Duguet, E. Design and Synthesis of Janus Micro- And Nanoparticles. *J. Mater. Chem.* **2005**, *15*, 3745–3760.
13. Glotzer, S. C. Some Assembly Required. *Science* **2004**, *306*, 419–420.
14. Paunov, V. N.; Cayre, O. J. Supraparticles and Janus Particles Fabricated by Replication of Particle Monolayers at Liquid Surfaces Using a Gel Trapping Technique. *Adv. Mater.* **2004**, *16*, 788–791.
15. Bulusu, S.; Li, X.; Wang, L-S.; Zeng, X. C. Evidence of Hollow Golden Cages. *Proc. Natl. Acad. Sci.U.S.A.* **2006**, *103*, 8326–8330.
16. Li, J.; Li, X.; Zhai, H-J.; and Wang, L-S. Au_{20}: A Tetrahedral Cluster. *Science* **2003**, *299*, 864–867.
17. Ji, M.; Gu, X.; Li, X.; Gong, X. G.; Li, J.; Wang, L. S. Experimental and Theoretical Investigation of the Electronic and Geometrical Structures of the Au_{32} Cluster. *Angew. Chem., Int. Ed.* **2005**, *44*, 7119–7123.
18. Gu, X.; Ji, M.; Wei, S. H.; Gong, X. G. Au_N Clusters ($N = 32$, 33, 34, 35): Cagelike Structures of Pure Metal Atoms. *Phys. Rev. B* **2004**, *70*, 205401.
19. Sun, Q.; Wang, Q.; Rao, B. K.; Jena, P. Electronic Structure and Bonding of Au on a SiO_2 Cluster: A Nanobullet for Tumors. *Phys. Rev. Lett.* **2004**, *93*, 186803.
20. Sun, Q.; Jena, P.; Kim, Y. D.; Fischer, M.; Gantefor, G. Interactions of Au Cluster Anions with Oxygen. *J. Chem. Phys.* **2004**, *120*, 6510–6515.

21. Sun, Q.; Reddy, B. V.; Marquez, M.; Jena, P.; Gonzalez, G.; Wang, Q. Theoretical Study on Gold-Coated Iron Oxide Nanostructure: Magnetism and Bioselectivity for Amino Acids. *J. Phys. Chem. C* **2007**, *111*, 4159–4163.
22. Sun, Q.; Kandalam, A. K.; Wang, Q.; Jena, P.; Kawazoe, Y.; and Marquez, M. Effect of Au Coating on the Magnetic and Structural Properties of Fe Nanoclusters for Use in Biomedical Applications: A Density-Functional Theory Study. *Phys. Rev. B* **2006**, *73*, 134409.
23. Sun, Y-G.; Xia, Y-N. Shape-Controlled Synthesis of Gold and Silver Nanoparticles. *Science* **2002**, *298*, 2176–2179.
24. Mokari, T.; Rothenberg, E.; Popov, I.; Costi, R.; Banin, U. Selective Growth of Metal Tips onto Semiconductor Quantum Rods and Tetrapods. *Science* **2004**, *304*, 1787–1790.
25. Shankar, S. S.; Rai, A.; Ankamwar, B.; Singh, A.; Ahmad, A.; Sastry, M. Biological Synthesis of Triangular Gold Nanoprisms. *Nat. Mater.* **2004**, *3*, 482–488.
26. Darbha, G. K.; Ray, A.; Ray, P. C. Gold Nanoparticle-Based Miniaturized Nanomaterial Surface Energy Transfer Probe for Rapid and Ultrasensitive Detection of Mercury in Soil, Water, And Fish. *ACS Nano* **2007**, *1*, 208–214.
27. Chen, S.; Wang, Z. L.; Ballato, J.; Foulger, S. H.; Carroll, D. L. Monopod, Bipod, Tripod, And Tetrapod Gold Nanocrystals. *J. Am. Chem. Soc.* **2003**, *125*, 16186–16187.
28. Jana, N. R.; Gearheart, L.; Murphy, C. J. Wet Chemical Synthesis of High Aspect Ratio Cylindrical Gold Nanorods. *J. Phys. Chem. B* **2001**, *105*, 4065–4067.
29. Malikova, N.; Pastoriza-Santos, I.; Schierhorn, M.; Kotov, N. A.; Liz-Marzan, L. M. Layer-by-Layer Assembled Mixed Spherical and Planar Gold Nanoparticles: Control of Interparticle Interactions. *Langmuir* **2002**, *18*, 3694–3697.
30. Pyykko, P.; Runeberg, N. Icosahedral WAu_{12}: A Predicted Closed-Shell Species, Stabilized by Aurophilic Attraction and Relativity and in Accord with the 18-Electron Rule. *Angew. Chem., Int. Ed.* **2002**, *41*, 2174–2176.
31. Li, X.; Kiran, B.; Li, J.; Zhai, H.-J.; Wang, L.-S. Experimental Observation and Confirmation of Icosahedral $W@Au_{12}$ and $Mo@Au_{12}$ Molecules. *Angew. Chem., Int. Ed.* **2002**, *41*, 4786–4789.
32. Autschbach, J.; Hess, B. A.; Johansson, M. P.; Neugebauer, J.; Patzschke, M.; Pyykko, P.; Reiher, M.; Sundholm, D. Properties of WAu_{12}. *Phys. Chem. Chem. Phys.* **2004**, *6*, 11–22.
33. Manninen, K.; Pyykko, P.; Hakkinena, H. A Small Spherical Liquid: A DFT Molecular Dynamics Study of WAu_{12}. *Phys. Chem. Chem. Phys.* **2005**, *7*, 2208–2211.
34. Knight, W. D.; Clemenger, K.; de Heer, W. A.; Saunders, W. A.; Chou, M. Y.; Cohen, M. L. Electronic Shell Structure and Abundances of Sodium Clusters. *Phys. Rev. Lett.* **1984**, *52*, 2141–2143.
35. Samanta, C.; Adhikari, S. Shell Effect in Pb Isotopes near the Proton Drip Line. *Nucl. Phys. A* **2004**, *738*, 491–494.
36. Gubbs, R. B. Nanoparticle Asembly Solvent-Tuned Structures. *Nat. Mater.* **2007**, *6*, 553–556.
37. Nie, Z.; Fava, D.; Kumacheva, E.; Zou, S.; Walker, G. C.; Rubinstein, M. Self-Assembly of Metal-Polymer Analogues of Amphiphilic Triblock Copolymers. *Nat. Mater.* **2007**, *6*, 609–614.
38. Teo, B. K.; Zhang, H. Clusters of Clusters: Self-Organization and Self-Similarity in the Intermediate Stages of Cluster Growth of Au-Ag Supraclusters. *Proc. Natl. Acad. Sci. U.S.A.* **1991**, *88*, 5067–5071.
39. Nobusada, K.; Iwasa, T. Oligomeric Gold Clusters with Vertex-Sharing Bi- And Triicosahedral Structures. *J. Phys. Chem. C* **2007**, *111*, 14279–14282.
40. Nose, S. Unified Formulation of the Constant Temperature Molecular Dynamics Methods. *J. Chem. Phys.* **1984**, *81*, 511–519.
41. Kresse, G.; Joubert, J. From Ultrasoft Pseudopotentials to the Projector Augmented-Wave Method. *Phys. Rev. B* **1999**, *59*, 1758–1775.
42. Kresse, G.; Furthmüller, J. Efficient Iterative Schemes for ab Initio Total-Energy Calculations Using a Plane-Wave Basis Set. *Phys. Rev. B* **1996**, *54*, 11169–11186.
43. Sun, Q.; Wang, Q.; Kawazoe, Y.; Jena, P. Interaction of Magic Gold Cluster with Si_{60} Cage. *Eur. Phys. J. D* **2004**, *29*, 231–234.
44. Sun, Q.; Wang, Q.; Jena, P.; Note, R.; Yu, J-Z.; Kawazoe, Y. Metastability of a Gold Nanoring: Density-Functional Calculations. *Phys. Rev. B* **2004**, *70*, 245411.
45. Sun, Q.; Wang, Q.; Chen, G.; Jena, P. Structure of $SiAu_{16}$. *J. Chem. Phys.* **2007**, *127*, 214706–214709.